ChemRxiv™

doi.org/10.26434/chemrxiv.10119230.v1

Strain Induced Tunability of the Electronic Properties of SrTiO3 Interfaces

Zhenyun Lan, Tejs Vegge, Ivano E. Castelli

Submitted date: 01/11/2019 • Posted date: 20/11/2019

Licence: CC BY-NC-ND 4.0

Citation information: Lan, Zhenyun; Vegge, Tejs; Castelli, Ivano E. (2019): Strain Induced Tunability of the Electronic Properties of SrTiO3 Interfaces. ChemRxiv. Preprint.
https://doi.org/10.26434/chemrxiv.10119230.v1

SrTiO 3 (STO) films are widely used as substrates in oxide devices. Although STO is one of the most studied materials, both experimentally and computationally, the effect of strain at the interface is almost completely ignored. In this work, we perform Density Functional Theory (DFT) calculations using the SCAN meta-GGA exchange-correlation functional to study the effect of uniaxial- and biaxial-strain on structural and electronic properties of STO interfaces. We find that under tensile uniaxial-strain, the band gap increases significantly, as a consequence of a large tilting in the octahedra. On the other side, under compression, the band gap is almost constant. Similar effects are seen for tensile biaxial strain, while for compressive strain, the gap first increases and then decreases, due to the temporary appearance of a polar distortion. In addition, we observe an orbital inversion at the conduction-band edge under different uni/bi-axial-strain conditions. This work provides a new perspective of the use of strain to modulate the structural and electronic properties of perovskite film materials for multiple applications.

File list (1)

Strain_in_STO(4).pdf (11.14 MiB) view on ChemRxiv • download file

Strain Induced Tunability of the Electronic Properties of $SrTiO_3$ Thin Films

Zhenyun Lan, Tejs Vegge, and Ivano E. Castelli*
Department of Energy Conversion and Storage, Technical University of Denmark, Fysikvej 309, DK-2800 Kgs. Lyngby, Denmark
(Dated: November 8, 2019)

$SrTiO_3$ (STO) films are widely used as substrate of oxide devices. Although STO is one of the most studied materials, both experimentally and computationally, the effect of strain at the interface is almost completely ignored. In this work, we perform Density Functional Theory (DFT) calculations using the SCAN meta-GGA exchange-correlation functional to study the effect of uniaxial- and biaxial-strain on structural and electronic properties of STO interfaces. We find that under tensile uniaxial-strain, the band gap increases significantly, as a consequence of a large tilting in the octahedra. On the other side, under compression, the band gap is almost constant. Similar effects are seen for tensile biaxial strain, while for compressive strain, the gap first increases and then decreases, due to the temporary appearance of a polar distortion. In addition, we observe an orbital inversion at the conduction-band edge under different uni/bi-axial-strain conditions. This work provides a new perspective of the use of strain to modulate the structural and electronic properties of perovskite film materials for multiple applications.

I. INTRODUCTION

Strontium titanate ($SrTiO_3$, STO), one of the most studied perovskites, is a key material with the unique physical properties, such as photocatalytic ability for water splitting, strain-induced ferroelectricity, a two-dimensional electron gas behavior at the (001) surface, which has been widely applied in several areas and devices.[1–6] The tunable electronic structures render it a promising semiconductor in optical related field. Furthermore, as a semiconductor, its electronic structure properties largely depends on the crystal structure, such as unit cell parameter, tilting of the octahedra, crystal symmetry and so on. This can be achieved in different ways, from defects to applied external strain.

Benefiting from improvements in synthesis techniques, STO films with specific thickness have been fabricated, which have pioneered the use of STO for applications in a broad range of technological fields, such as electronics, catalysis, optics and superconductivity. At the same time, STO slab has also been extensively investigated by means of atomic scale simulations to investigate bulk and surface properties. For example, Padilla *et al.* showed that the electronic structures of two possible terminations of STO (001) surfaces are different, i.e. the band gap for the TiO_2-terminated surface is smaller than the one of the SrO-terminated STO.[7] Pojani and co-authors discussed the polarity effects at the (111) and (110) surfaces in STO.[8] Guo and co-authors found that anion-doping can influence the surface structure, the electronic structure and the photocatalytic performance of the STO(001) surface with different terminations.[9]

In the most controlled form, strain engineering can be efficiently used to modulate the crystal structure, as a pathway to control the physical properties of materials.[10–12] In the past years, many theoretical works have been devoted to study the influence that strain has on the properties of STO. For example, Zhou *et al.* have carried out a comprehensive investigation of the effects of strain on thermoelectric properties of STO.[13] Janotti and co-authors found that the strain will influence the electron mobility of STO.[14] Strain-driven phase transition in incipient ferroelectric STO was observed by Ni *et al.*.[15] In comparison to biaxial strain, uniaxial strain changes significantly the crystal structure because of a breaking of the symmetry, which is followed by interesting properties such as band splitting in STO.[16] Many studies of 2D materials under uniaxial strain have also been reported. A band gap tuning in monolayer $MoSe_2$ by uniaxial strain was report by Island *et al.*.[17] Li and co-author reported giant anisotropic Raman response of encapsulated ultrathin black phosphorus by uniaixal strain. The Raman shift rates of the A_g^1, B_{2g}, and A_g^2 modes are significantly distinct for strain applied along different directions.[18]

Despite these interesting effects, most of the computational work on strained materials is performed on the bulk (3D) structure, neglecting the effects that strain has on the surface. In this work, we study the effects that uni- and bi-axial strain has on structural and electronic properties on a STO slab.

II. COMPUTATIONAL METHODS

All calculations were performed in the framework of Density Functional Theory (DFT) using the strongly constrained and appropriately normed (SCAN) meta-GGA exchange-correlation functional as implemented in the Vienna ab-initio simulation package (VASP).[19, 20] SCAN often yields an accuracy comparable to or better than hybrid GGAs, almost at the cost of a GGA calculation, and without using a Hubbard U correction.[21–23] We note that although the electronic occupation is calcu-

* ivca@dtu.dk

lated correctly using SCAN, the values of the band gap are underestimated. Despite this, trends and correlations are still valid. As this is the main focus of the paper and more accurate calculations, such as GW method or HSE06 functional, are too demanding, we are satisfied with the results obtained at the SCAN level of accuracy. The Brillouin zone was sampled with a $8 \times 8 \times 1$ Γ - centered k-point grid for the $1 \times 1 \times 5.5$ slab. A plane wave cutoff of 870 eV was used. The structure was optimized until the force on each atom was less than 0.01 eV/Å. The slabs were terminated by TiO_2. A vacuum of 20 Åwas applied to avoid the interaction between two images.

To better qualify the distortion in the octahedra, we calculate the polar distortion of each TiO_2 layer, δ_i, defined as follows:

$$\delta_i = \sqrt{\delta_x^2 + \delta_y^2}, \quad \text{with} \quad \delta_{x,y} = \overline{\delta}_{x,y}(Ti) - \overline{\delta}_{x,y}(O), \quad (1)$$

where $\overline{\delta}_i$ is the layer-averaged atomic displacement in TiO_2 layer relative to ideal cubic lattice.

Although, in this work, we consider a slab composed of $1 \times 1 \times 5.5$ unit cells, similar structural distortions and electronic properties are observed for a larger $2 \times 2 \times 5.5$ slab.

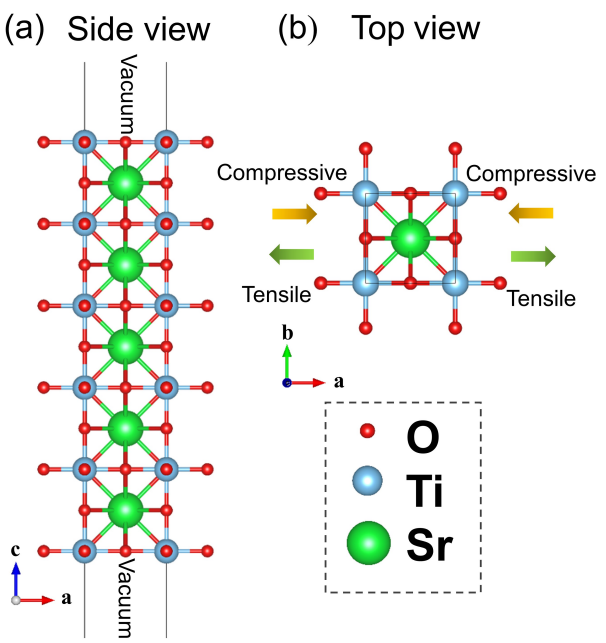

FIG. 1. (a) side view and (b) top view of the STO slab used here.

III. RESULTS AND DISCUSSION

A. Uniaxial Strain

Figure 1 shows the crystal structure of TiO_2-terminated $1 \times 1 \times 5.5$ STO slab. As a starting point, we consider the cubic structure, with the space group $Pm\bar{3}m$, as this phase is a typical representative of bulk STO at room temperature. The optimized lattice constant of bulk STO is a = 3.906 Å, which agrees well with experimental results (a = 3.906 Å).[24] Cleaving bulk STO in [001] direction, a $1 \times 1 \times 5.5$ STO slab with two TiO_2 terminations is built. The lattice constant for optimized STO slab is a=b=3.886 Å, which is slightly smaller compared to bulk value. This is however in good agreement with previous literature.[25] Uniaxial strain is applied in the [100] direction. The uniaxial strain is defined as ε_u=(a-a_0)/a_0×100%, $where a_0$ is the lattice constant of fully optimized STO slab (without strain) and a is the lattice constant of the structure with strain. The lattice constants in the [010] and [001] directions and the atomic positions are allowed to fully relax, keeping the [001] direction fixed under a certain strain value.

Figure 2(a) shows the band gap of STO as a function of the applied strain: the band gap is almost not influenced by a compressive strain, which is almost constant at a value of about 0.9 eV. The band gap is again almost constant for a tensile strain up to 1 %, but afterwards, between 1 and 2 % increases of 0.3 eV. Even further, the band gap of STO continues to increase linearly with the increase of the strain after 2 %. A phase transition has been observed between 1 and 2 %, which is directly responsible for the abrupt change in the gap. This phase changes mostly involve a distortion in the octahedra. Without any applied strain, the angle for O-Ti-O, averaged among the six TiO_2 layers, is 90.0°, as expected by the cubic symmetry. However, under 2% tensile strain, the average angle reduces to 86.6°, as schematized in the insets of Figure 2(a). The uniaxial strain, compressive and tensile, has thus different effects on the band structures because of a change of the crystallographic symmetry.

This can be further seen by investigating the positions of band edges as a function of the strain (Figure 2(b)). Under compressive strain, both conduction band and valence band drift simultaneously, with their difference almost unchanged, i.e. the gap does not vary. Under tensile strain and after the phase transition, the conduction band edge shift-up linearly and significantly more than the valence band. This has the effect of increasing the band gap. Figure 2(c) shows the Projected Density of States (PDOS) for 2% compressive, 0 and 2% tensile strain: the O p orbitals mainly contribute to the valence band maximum (VBM), and the conduction band minimum (CBM) is mainly consist of Ti d orbitals. At the electronic level, the Ti orbitals are thus the main responsible for the increase of the gap as a function of the strain.

The change of the order of the Ti $3d$ orbitals at the CBM are presented in Figure 2(d): the Ti $3d_{xy}$ orbitals are the main component of the valence band edge for unstrained STO. On the surface, in fact, the cubic symmetry is broken in the z-direction, which also breaks the degeneracy of t_{2g} orbitals and thus the $3d_{xy}$

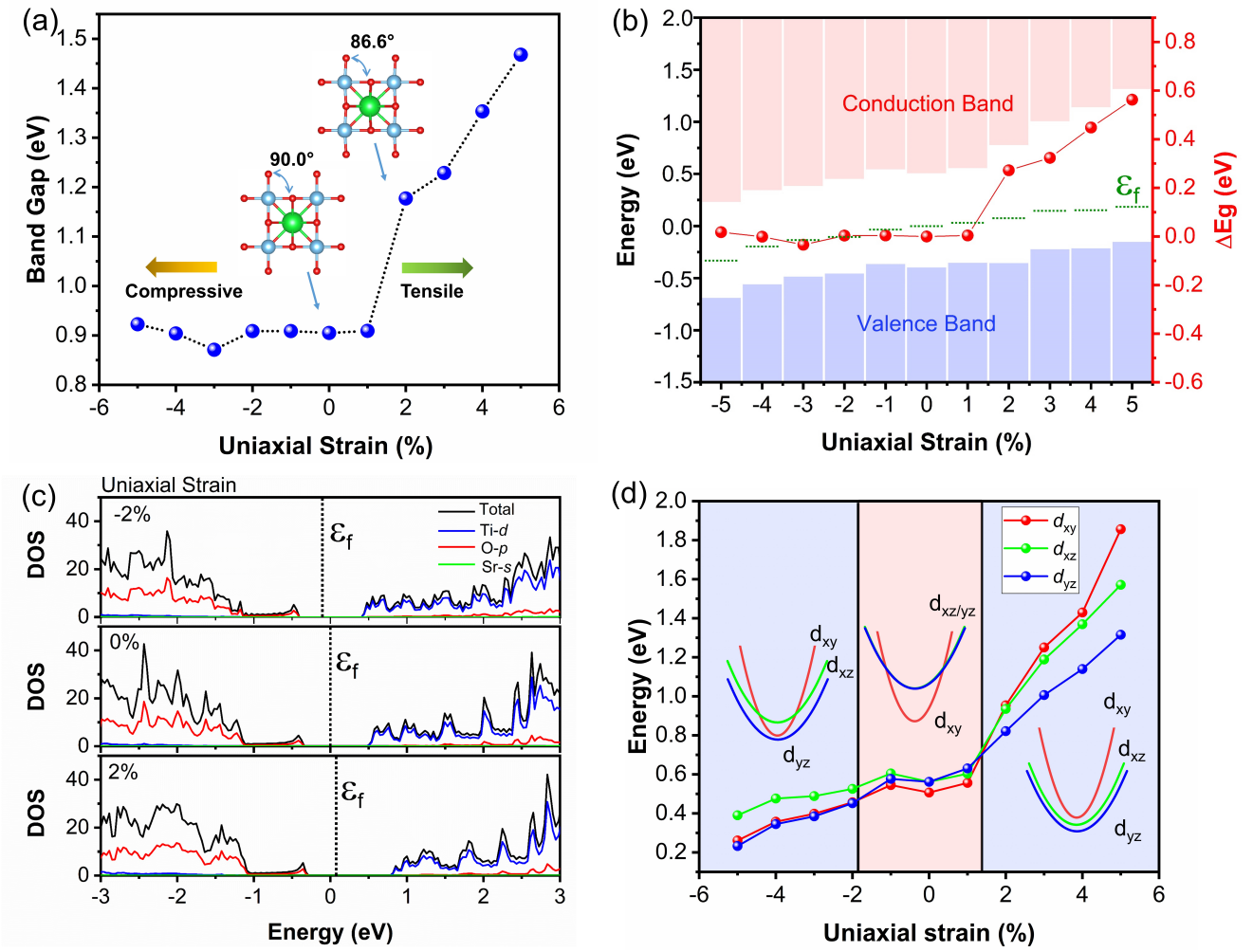

FIG. 2. (a) The band gap of STO slab as a function of strain. The insert figures represent the top view of STO slab structure under 0 and 2 % uniaxial tensile strain, respectively. (b) Band edge positions and the changes of band gap ($\triangle E = Eg - Eg_0$, Eg_0 is the band gap of unstrained STO slab, E_g is the band gap of STO slab at a certain strain) for STO slab as a function of uniaxial strain. The relative positions of the band edges of the strianed STO with reference to vacuum level of unstrained STO. And the work function for unstrained STO slab is 5.36 eV. The green dash lines represent the positions of fermi level at different states. (c) Total and projected density of states for STO slab with 2% uniaxial compressive strain, 0 uniaxial strain and 2 % uniaxial tensile strain, respectively. The fermi level for unstrained STO is set as 0 eV. (d) Ti $3d_{xy}$, $3d_{xz}$ and $3d_{yz}$ orbitals positions for STO slab under different unaxial strain. Three regions from left to right can be identified as $3d_{yz}$ dominated area, $3d_{xy}$ orbitals dominated area and $3d_{yz}$ orbitals dominated area, respectively.

orbitals have the lowest energy. The energy of Ti $3d_{xy}$ and $3d_{xz}$ orbitals increase/decrease significantly, under tensile/compressive strain and now the Ti $3d_{yz}$ orbitals are the main component of the CBM.

The polar distortions in six atom layers are calculated to define the octahedral tilt, as shown in Figure 3. Under compressive strain, there is no polar distortion, while under tensile strain, a significantly increase of the average value of polar distortion from 0 Åto 0.12 Åfor 2 % tensile strain is observed and it continues to increase for larger applied strain.

B. Biaxial Strain

The biaxial strain is applied in the xy-plane, perpendicular to the [001] interface. The magnitude of the strain is now defined as ε_b=(a-a_0)/a_0 × 100 %, where a is the lattice constant in both [100] and [010] directions. The atomic positions are allowed to relax, keeping the unit cell fixed. As shown in Figure 4(a), under tensile strain above 1 %, the band gap increases significantly, which is very similar to what happens under tensile uniaxial-strain. This is again connected with a change of the symmetry. Differently from the case of uniaxial-strain, for biaxial-strain, the polar distortion directions in six

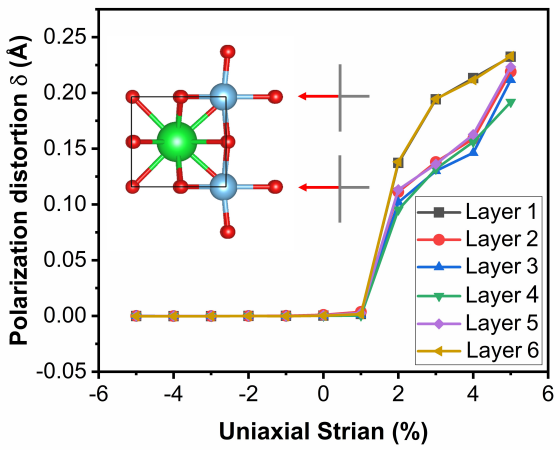

FIG. 3. The polar distortion value in six TiO_2 atom layers as a function of uniaxial strain. The insert is the top view of STO slab. (The polar distortion direction is marked by the red arrow.)

atom layers of STO slab change, as shown in Figure 4(b). The polar distortion appears at a tensile strain above 2 %. For each layer, the energy difference for the polar distortions in the $[\bar{1}\ \bar{1}0]$ or $[\bar{1}10]$ (marked with a red arrow in figure) is below the accuracy achievable with DFT. Under compressive strain, the band gap firstly increases (between 0 and 1 %) and then decreases linearly with the increase of the strain. This tendency is very different from compressive uniaxial-strain, where the gap is almost constant. The reason for the increase of the gap between 0 and 1 % compressive strain could be related with the small polar distortions that is observed at small compressive strain. Once that the strain increases, the polar distortion disappear as a consequence of the increased internal pressure. Figure 4 (c) shows the change of the band gap and positions of the band edges as a function of the strain. Compared to the uniaxial-strain, where the VBM edge and the CBM edge decrease similarly, in the compressive biaxial-strain case, decrease of the CBM edge is larger than the decrease of the VBM edge, resulting in a decrease of band gap.

As shown in Figure 4 (d), the contribution to CBM changes from Ti $3d_{xy}$ orbitals to $3d_{yz}$ orbitals when applying compressive/tensile biaxial strain larger than 2%. Under compressive strain, the energy of $3d_{xz}$ and $3d_{yz}$ are similar, i.e. the degeneracy is not broken. While, under tensile strain, the energy of $3d_{xz}$ and $3d_{yz}$ orbitals are different due to a broken symmetry.

C. Implication for functional materials

Strain on thin films can pave the way to functionalize materials for multiple applications. Compared to strain applied to bulk materials, for which the band gap increase gradually under both compressive and tensile biaxial strain, our results show that the band gap and other electronic properties can be tuned in many different ways.[26] To achieve this, it is necessary to investigate the properties of slab surfaces, beyond the bulk models.

The effect of strain on the electronic properties can boost the potential applications of this-films for electronic devices. Experimentally, uniaxial strain can be induced, for example, by bending a STO slab on a polymeric support. Uniaxial strain has been applied to La doped STO film in a three-point bending apparatus. And they observed an large enhancements of electron mobilities under uniaxial stress.[27] Biaxial strain can also be induced by epitaxial growth, as it has been performed by Haeni and co-authors.[28] The challenge for the computational community is thus to select the optimal matching to achieve the target strain in the thin-film material.[29]

More in general, it has been recently discussed that strain and nano-confinement can be two possible pathways to stabilize metastable materials and interfaces.[30] Calculations similar to the ones performed in this work are required, to achieve this goal and to design optimal pathways to guide experiments.

To ensure reproducibility of the results, all input and output from the calculations and the scripts used to run the simulations are available on the open-source database Computational Materials Repository (CMR) at the date of publication.[31]

IV. CONCLUSION

In summary, we have used DFT calculations to investigate the structural and electronic properties of STO slab under uni- and bi-axial strain. We found that STO slab shows a different response for the structural-electronic properties under different strain conditions. The band gap increases significantly above 2% uni- and bi-axial tensile strain, which is due to a lager octahedral tilt. Under compressive strain, the gap is constant for uniaxial strain, while it increases firstly and then decreases for biaxial strain. An orbital inversion is observed: the contribution to the CBM changes from Ti d_{xy} orbitals to Ti d_{yz} orbitals. Our results demonstrate that the uni- and biaxial-strain on STO slab is different from that of STO bulk. Therefore, the methodology discussed in this work can be a reference to investigate uni- and bi-axial strain on other thin-film materials.

ACKNOWLEDGMENTS

ZL acknowledge support from the China Scholarship Council (CSC). TV and IEC wish to acknowledge the support from the Department of Energy Conversion and Storage, Technical University of Denmark, through the Special Competence Initiative Autonomous Materials Discovery (AiMade).

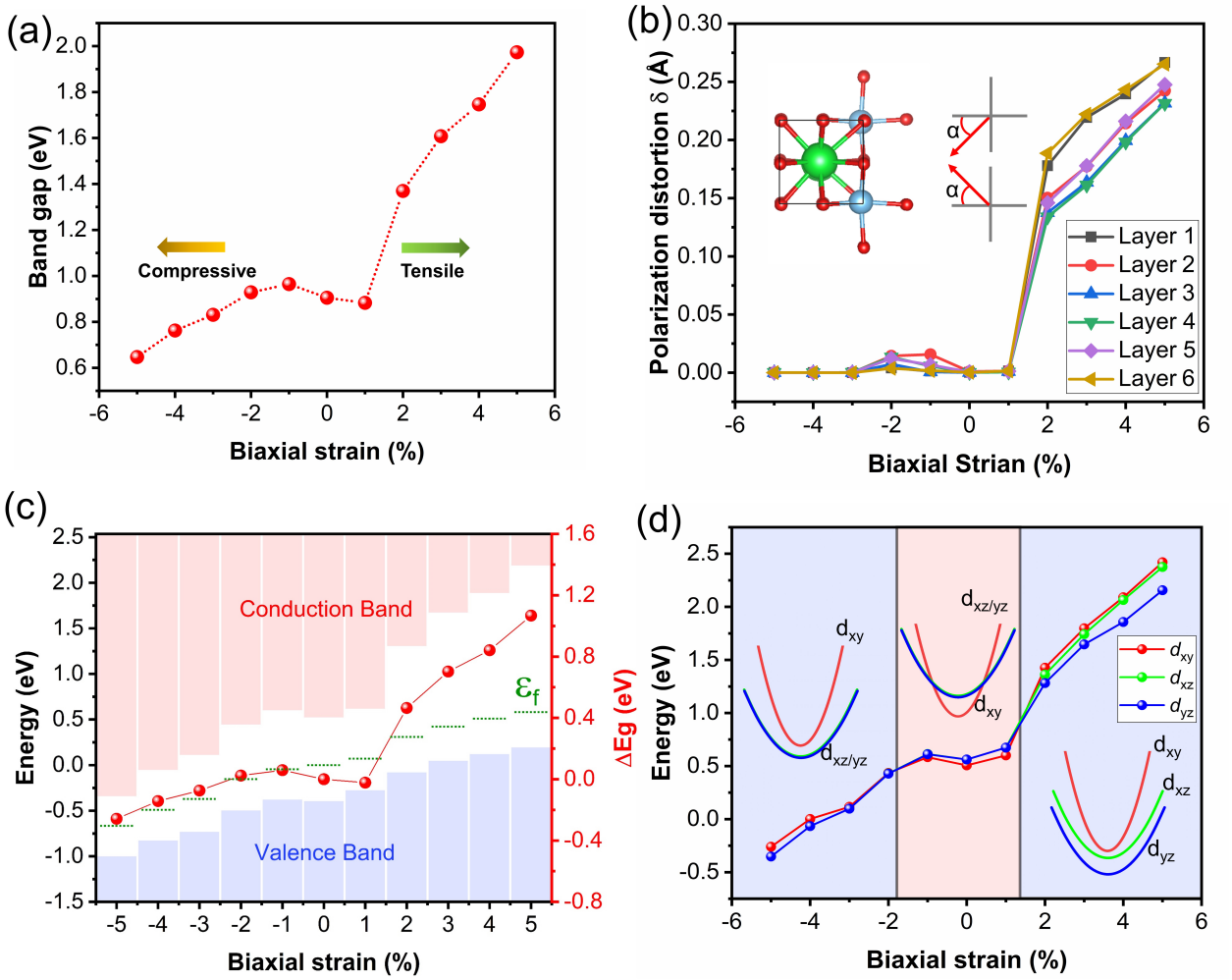

FIG. 4. (a) The band gap of STO slab as a function of biaxial strain. (b) The values of polar distortion in six TiO_2 atom layers as a function of biaxial strain. (The polar distortion directions are marked by the red arrows. α is about 45°) (c) Band edge positions and the changes of band gap ($\triangle E = Eg - Eg_0$, Eg_0 is the band gap of unstrained STO slab, E_g is the band gap of STO slab at a certain strain) for STO slab as a function of biaxial strain.The relative positions of the band edges of the strianed STO with reference to vacuum level of the unstrained STO. The green dash lines represent the positions of fermi level at different states. (d) Ti $3d_{xy}$, $3d_{xz}$ and $3d_{yz}$ orbitals positions for STO slab under different biaxial strain. Three regions from left to right can be identified as $3d_{xz/yz}$ dominated area, $3d_{xy}$ orbitals dominated area and $3d_{yz}$ orbitals dominated area, respectively.

[1] K. Iwashina and A. Kudo, Rh-doped srtio3 photocatalyst electrode showing cathodic photocurrent for water splitting under visible-light irradiation, Journal of the American Chemical Society **133**, 13272 (2011).

[2] B. Wang, S. Shen, and L. Guo, Surface reconstruction of facet-functionalized srtio3 nanocrystals for photocatalytic hydrogen evolution, ChemCatChem **8**, 798 (2016).

[3] A. Verma, S. Raghavan, S. Stemmer, and D. Jena, Ferroelectric transition in compressively strained srtio3 thin films, Applied Physics Letters **107**, 192908 (2015).

[4] R. Wördenweber, E. Hollmann, R. Kutzner, and J. Schubert, Induced ferroelectricity in strained epitaxial srtio 3 films on various substrates, Journal of applied physics **102**, 044119 (2007).

[5] S. M. Walker, F. Y. Bruno, Z. Wang, A. De La Torre, S. Riccó, A. Tamai, T. K. Kim, M. Hoesch, M. Shi, M. S. Bahramy, *et al.*, Carrier-density control of the srtio3 (001) surface 2d electron gas studied by arpes, Advanced Materials **27**, 3894 (2015).

[6] P. Delugas, V. Fiorentini, A. Mattoni, and A. Filippetti, Intrinsic origin of two-dimensional electron gas at the

(001) surface of srtio 3, Physical Review B **91**, 115315 (2015).
[7] J. Padilla and D. Vanderbilt, Ab initio study of srtio3 surfaces, Surface Science **418**, 64 (1998).
[8] A. Pojani, F. Finocchi, and C. Noguera, Polarity on the srtio3 (111) and (110) surfaces, Surface Science **442**, 179 (1999).
[9] Y. Guo, X. Qiu, H. Dong, and X. Zhou, Trends in nonmetal doping of the srtio 3 surface: a hybrid density functional study, Physical Chemistry Chemical Physics **17**, 21611 (2015).
[10] N. Vonrüti and U. Aschauer, Band-gap engineering in ab (o x s 1- x) 3 perovskite oxysulfides: a route to strongly polar materials for photocatalytic water splitting, Journal of Materials Chemistry A (2019).
[11] J. Guan, W. Song, L. Yang, and D. Tománek, Strain-controlled fundamental gap and structure of bulk black phosphorus, Physical Review B **94**, 045414 (2016).
[12] C. Grote and R. F. Berger, Strain tuning of tin–halide and lead–halide perovskites: a first-principles atomic and electronic structure study, The Journal of Physical Chemistry C **119**, 22832 (2015).
[13] D. Zou, Y. Liu, S. Xie, J. Lin, and J. Li, Effect of strain on thermoelectric properties of srtio3: First-principles calculations, Chemical Physics Letters **586**, 159 (2013).
[14] A. Janotti, D. Steiauf, and C. Van de Walle, Strain effects on the electronic structure of srtio 3: Toward high electron mobilities, Physical Review B **84**, 201304 (2011).
[15] L. Ni, Y. Liu, C. Song, W. Wang, G. Han, and Y. Ge, First-principle study of strain-driven phase transition in incipient ferroelectric srtio3, Physica B: Condensed Matter **406**, 4145 (2011).
[16] Y. J. Chang, G. Khalsa, L. Moreschini, A. L. Walter, A. Bostwick, K. Horn, A. H. MacDonald, and E. Rotenberg, Uniaxial strain induced band splitting in semiconducting srtio 3, Physical Review B **87**, 115212 (2013).
[17] J. O. Island, A. Kuc, E. H. Diependaal, R. Bratschitsch, H. S. van der Zant, T. Heine, and A. Castellanos-Gomez, Precise and reversible band gap tuning in single-layer mose 2 by uniaxial strain, Nanoscale **8**, 2589 (2016).
[18] Y. Li, Z. Hu, S. Lin, S. K. Lai, W. Ji, and S. P. Lau, Giant anisotropic raman response of encapsulated ultrathin black phosphorus by uniaxial strain, Advanced Functional Materials **27**, 1600986 (2017).
[19] J. Sun, A. Ruzsinszky, and J. P. Perdew, Strongly constrained and appropriately normed semilocal density functional, Physical review letters **115**, 036402 (2015).
[20] G. Kresse and J. Hafner, Ab initio molecular dynamics for liquid metals, Physical Review B **47**, 558 (1993).
[21] J. Sun, R. C. Remsing, Y. Zhang, Z. Sun, A. Ruzsinszky, H. Peng, Z. Yang, A. Paul, U. Waghmare, X. Wu, *et al.*, Accurate first-principles structures and energies of diversely bonded systems from an efficient density functional, Nature chemistry **8**, 831 (2016).
[22] M. Kaltak, M. Fernández-Serra, and M. S. Hybertsen, Charge localization and ordering in a 2 mn 8 o 16 hollandite group oxides: Impact of density functional theory approaches, Physical Review Materials **1**, 075401 (2017).
[23] V. I. Anisimov, J. Zaanen, and O. K. Andersen, Band theory and mott insulators: Hubbard u instead of stoner i, Physical Review B **44**, 943 (1991).
[24] L. Cao, E. Sozontov, and J. Zegenhagen, Cubic to tetragonal phase transition of srtio3 under epitaxial stress: An x-ray backscattering study, physica status solidi (a) **181**, 387 (2000).
[25] R. A. Èvarestov, *Theoretical modeling of inorganic nanostructures: Symmetry and ab-initio calculations of nanolayers, nanotubes and nanowires* (Springer, 2015).
[26] R. F. Berger, C. J. Fennie, and J. B. Neaton, Band gap and edge engineering via ferroic distortion and anisotropic strain: the case of srtio 3, Physical review letters **107**, 146804 (2011).
[27] B. Jalan, S. J. Allen, G. E. Beltz, P. Moetakef, and S. Stemmer, Enhancing the electron mobility of srtio 3 with strain, Applied Physics Letters **98**, 132102 (2011).
[28] J. Haeni, P. Irvin, W. Chang, R. Uecker, P. Reiche, Y. Li, S. Choudhury, W. Tian, M. Hawley, B. Craigo, *et al.*, Room-temperature ferroelectricity in strained srtio 3, Nature **430**, 758 (2004).
[29] H. Ding, S. S. Dwaraknath, L. Garten, P. Ndione, D. Ginley, and K. A. Persson, Computational approach for epitaxial polymorph stabilization through substrate selection, ACS Applied Materials & Interfaces **8**, 13086 (2016).
[30] V. Esposito and I. E. Castelli, Metastability at defective metal oxides interfaces and nanoconfined structures, under review Advanced Materials Interfaces **0**, 1 (2019).
[31] Computational materials repository (cmr), `http://cmr.fysik.dtu.dk`.
[32] Autonomous materials discovery (aimade), `http://www.aimade.org`.

Strain_in_STO(4).pdf (11.14 MiB) view on ChemRxiv • download file